PROF. DAVID CONWAY (Orcid ID : 0000-0002-8711-3037)

Article type : Original Article

Genome-wide mosaicism in divergence between zoonotic malaria parasite subpopulations with separate sympatric transmission cycles

Running title: zoonotic malaria parasite genome divergence

Paul C. S. Divis[1,2], Craig W. Duffy[2], Khamisah A. Kadir[1], Balbir Singh[1], David J. Conway[1,2]

[1] Malaria Research Centre, Faculty of Medicine and Health Sciences, Universiti Malaysia Sarawak, 94300 Kota Samarahan, Sarawak, Malaysia,

[2] Pathogen Molecular Biology Department, London School of Hygiene and Tropical Medicine, Keppel St, London WC1E 7HT, United Kingdom.

Corresponding author for proof checking: Prof David J. Conway david.conway@lshtm.ac.uk

Abstract

Plasmodium knowlesi is a significant cause of human malaria transmitted as a zoonosis from macaque reservoir hosts in Southeast Asia. Microsatellite genotyping has indicated that human infections in Malaysian Borneo are an admixture of two highly divergent sympatric parasite subpopulations that are respectively associated with long-tailed macaques (Cluster 1) and pig-tailed macaques (Cluster 2). Whole genome sequences of clinical isolates subsequently confirmed the separate clusters, although fewer of the less common Cluster 2 type were sequenced. Here, to analyse population structure and genomic divergence in subpopulation samples of comparable depth, genome sequences were generated from 21 new clinical infections identified as Cluster 2 by microsatellite analysis, yielding a cumulative sample size for this subpopulation similar to that for Cluster 1. Profound heterogeneity in the level of inter-cluster divergence was distributed bimodally across the genome in long contiguous chromosomal blocks. Different mitochondrial genome clades were associated with the two major subpopulations, but limited exchange of haplotypes from one to the other was evident, as was also the case for the maternally-inherited apicoplast genome. These findings indicate deep divergence of the two sympatric *P. knowlesi* subpopulations, with introgression likely to have occurred recently. There is no evidence yet of specific adaptation at any introgressed locus, but the recombinant mosaic types offer enhanced diversity on which selection may operate in a currently changing landscape and human environment. Loci responsible for maintaining genetic isolation of the sympatric subpopulations need to be identified in the chromosomal regions showing fixed differences.

Keywords: Genomic divergence, introgression, host-specificity, adaptation

Introduction

The zoonotic malaria parasite *Plasmodium knowlesi* is a significant cause of human malaria in Southeast Asia. Although long known as a malaria parasite of long-tailed and pig-tailed macaques that could potentially infect humans (Coatney *et al.*, 1971), the first large focus of human cases was only detected approximately 15 years ago in Malaysian Borneo (Singh *et al.*, 2004). Since then, infections have been described from throughout Malaysia (Cox-Singh *et al.*, 2008; William *et al.*, 2013; Yusof *et al.*, 2014) and in almost all countries in Southeast Asia (Singh and Daneshvar, 2013). Indeed, *P. knowlesi* is now the most common cause of human malaria in Malaysia (Barber *et al.*, 2017), with infections capable of reaching very high parasitaemia and sometimes leading to the death of patients (Cox-Singh *et al.*, 2008; Daneshvar *et al.*, 2009; Rajahram *et al.*, 2016; Singh and Daneshvar, 2013; William *et al.*, 2011).

Multi-locus microsatellite genotyping analysis of *P. knowlesi* infections revealed that human infections in Malaysian Borneo comprise two major genetic subpopulations that are respectively associated with long-tailed and pig-tailed macaque reservoir hosts (Divis *et al.*, 2015), with significant divergence confirmed by whole-genome sequence analyses of parasites in human infections (Assefa *et al.*, 2015). In most areas of Malaysian Borneo, the number of human clinical infections of the parasite subpopulation type associated with long-tailed macaques (Cluster 1) is higher than those having the type associated with pig-tailed macaques (Cluster 2) (Divis *et al.*, 2017). Further analyses of additional samples has subsequently revealed a third divergent subpopulation of *P. knowlesi* (Cluster 3) on the mainland of Southeast Asia which includes Peninsular Malaysia (Divis *et al.*, 2017; Yusof *et al.*, 2016). So far, only *P. knowlesi* parasites of Cluster 3 have been studied in infections of laboratory monkeys (Assefa *et al.*, 2015), and one strain of this type has been adapted to efficiently invade human erythrocytes in culture (Lim *et al.*, 2013; Moon *et al.*, 2013). To develop laboratory studies on the other two major zoonotic populations will require establishment of parasite isolates in controlled monkey infections, or ideally into culture with erythrocytes. Isolation of new *P. knowlesi* samples from human clinical infections is relatively straightforward, as most of these are not mixed with other species, whereas most natural *P. knowlesi* infections in macaques occur together with other primate malaria parasite species (Lee *et al.*, 2011).

The first large scale whole genome sequence analysis of *P. knowlesi* infections contained clinical samples that were mostly of the Cluster 1 type (N =38), yielding results indicating that this has undergone long-term population growth, with additional evidence of selection on particular loci (Assefa *et al.*, 2015). There were only ten Cluster 2 type infections sequenced in the study, which limited investigation of the demographic history of that subpopulation, but these were sufficient to indicate that the level of inter-cluster divergence varied across the genome, some loci having a concentration of apparently fixed differences and others showing more shared polymorphism (Assefa *et al.*, 2015). A separate simultaneous study reported data from another six infections, confirming the divergence between sympatric subpopulations (Pinheiro *et al.*, 2015), but this did not cumulatively give a much deeper sample. In agreement with the initial study (Assefa *et al.*, 2015), a recent secondary analysis of the previously published data confirmed the existence of genomic regions with shared polymorphisms (Diez Benavente *et al.*, 2017), but did not include any new data.

For a more informed comparison of these important zoonotic parasite subpopulations, a much larger sample of Cluster 2 type *P. knowlesi* genome sequences was obtained in this study. Combining the new data with samples sequenced previously (Assefa *et al.*, 2015; Pinheiro *et al.*, 2015) yielded a total of 34 Cluster 2 genome sequences that enables a more comprehensive analysis of genomic polymorphism and divergence between the subpopulations. This provides new understanding on the genome-wide variation in divergence of these two sympatric *P. knowlesi* subpopulations, essential for understanding their long term maintenance and potential for future adaptation.

Materials and Methods

New *P. knowlesi* DNA samples selected for analysis

Venous blood samples were obtained from patients infected with *P. knowlesi* malaria at Kapit Hospital in Sarawak between March and November 2014, after written informed consent from each patient had been obtained. The collection of blood samples was approved by the Medical Research and Ethics Committee of the Malaysian Ministry of Health, and by the Ethics Committee of the London School of Hygiene and Tropical Medicine. Leukocytes were removed by allowing 10 ml of blood to pass through a CF11 cellulose column, to enrich for erythrocytes and thereby increase the proportion of parasite compared to host DNA. Genomic DNA was extracted using QIAamp DNA Mini kits (QIAGEN, Germany), and all infections were confirmed to contain only *P. knowlesi* by nested PCR assays testing for all locally known malaria parasite species (Lee *et al.*, 2011). Determination of the genetic subpopulation cluster of each DNA sample was conducted by microsatellite genotyping (Divis *et al.*, 2017), and 21 samples of the Cluster 2 type that had sufficient DNA were selected for whole-genome sequencing. These were mostly single genotype infections as determined by microsatellite typing (Divis *et al.*, 2017).

P. knowlesi whole genome sequencing

DNA libraries were constructed using the TruSeq Nano DNA Library Preparation Kit (Illumina, San Diego, CA, USA). Physical shearing of the genomic DNA into fragments having an average size of 550 bp was performed using a M220 Focused-ultrasonicator (Covaris, USA). After denaturation at 95°C for 3 minutes, amplification of genomic DNA was performed with low number of PCR cycles (eight cycles at 98°C for 20 seconds, 60°C for 15 seconds and 72°C for 30 seconds) followed by a 72°C completion for 5 minutes. The quality of DNA libraries was assessed using the Agilent High Sensitivity DNA kit (Agilent Technologies, Santa Clara, CA US) while quantitation was done using the KAPA

Library Quantification Kit for Illumina® platform (KAPA Biosystems, Boston, MA, USA). All libraries were then normalised to 4 nM, and up to 12 samples were included on each sequencing run. Paired-end whole genome sequencing was performed on pooled DNA libraries using MiSeq Chemistry version 3 reagents, on the MiSeq platform (Illumina, San Diego, CA, USA) with a read length of 300 bp. Raw data of short reads generated in FASTQ format were undergone for quality check using the Trimmomatic software (Bolger *et al.*, 2014) with defined parameters (LEADING:3 TRAILING:3, SLIDINGWINDOW:4:10 MINLEN:36).

Trimmed FASTQ reads for individual isolates were then aligned against the version 2.0 of *P. knowlesi* strain H reference genome (www.genedb.org/Homepage/Pknowlesi, genome annotation March 2014, accessed December 2015) using the Burrows-Wheeler Aligner software version 0.7 with the BWA-MEM algorithm by default parameters (Li, 2013). This generated file in the SAM (sequence alignment/map) format, and followed by the conversion into a BAM (binary alignment/map) format using the SAMtools package version 0.1 (Li *et al.*, 2009). Due to the possible effect of PCR amplification bias introduced during the DNA library preparations, read duplications were removed using the '*MarkDuplicates*' command from the Picard toolkit (https://github.com/broadinstitute/picard). The average depth coverage was analysed by the BEDTools version 2 package using the '*genomeCoverageBed'* command (Quinlan and Hall, 2010).

Re-mapping of short read genome sequences generated from previous studies (Assefa *et al.*, 2015; Pinheiro *et al.*, 2015) against the version 2.0 of *P. knowlesi* strain H reference genome was also performed in the analysis (Table S1, Supporting information). These include 48 isolates from Kapit and Betong in Malaysian Borneo (Sequence Read Archive numbers ERR985372 – ERR985419) representing Cluster 1 and Cluster 2 type parasites collected between 2008 and 2013, six isolates from Sarikei in Malaysian Borneo (SRA numbers ERR274221, ERR274222, ERR274224, ERR272225, ERR366425 and ERR366426) and 5laboratory isolates (“Nuri” SRA numbers ERR019406, “Hackeri” SRR2221468, “Malayan” SRR2225467, “MR4-H” SRR2225571 and “Philippines” SRR2225573). The reference H strain sequence belongs to Cluster 3 (Assefa *et al.*, 2015), which is approximately equally divergent from Clusters 1 and 2, so no bias is expected in the efficiency of mapping of the sequences to this reference.

Single nucleotide polymorphism (SNP) calling and filtration

The calling of high quality SNPs was performed using several steps, following procedures described previously (Assefa *et al.*, 2015). For each isolate, SNPs were first identified from the BAM file using SAMTools/BCFTools with the following parameters: *mpileup –B –Q 23 –d 2000 –C 50 –ugf; varFilter –d 10 -D 2000*. This would generate a VCF (variant call format) file. A high-quality list of potential variant positions (Phred quality, Q > 30) were extracted from this file and a list of unique SNP lists were generated by concatenating all variant positions from all isolates. Using these unique SNP positions, the mapping quality (mq) and base quality (bq) were checked for each isolate to remove positions with an excess of low quality reads with the requirement of the minimum read depth coverage at 10x. The ratio of read depth values at high-quality (mq = 26; bq = 23) and low-quality (mq = 0; bq = 0) thresholds were calculated for each isolate using customised Perl scripts, and any SNP positions with the ratio below 0.5 were discarded.

Further filtration involved the removal of positions that contained ambiguous sequences (represented as a long stretch of unknown nucleotides ‘N’) in the reference genome. The *SICAVar*, *KIR*, and *pk-fam-a* to *pk-fam-e* multigene families (Pain *et al.*, 2008) and the subtelomeric regions were also filtered out to avoid ambiguous alignments which may cause false-positive SNP calls. Subtelomeric regions were here determined by visually inspecting the whole genome synteny mapping of *P. knowlesi* with the *P. vivax* homolog using the PlasmoDB GBrowse v2.48 (plasmodb.org/cg-bin/gbrowse/plasmodb/), with the boundaries of subtelomeric regions defined as sequences adjacent to the first conserved protein-coding gene (Table S2, Supporting information). After exclusion of subtelomeric regions and the large multigene families, 21.2 Mb (92%) of the 23.0 Mb corresponding to the reference nuclear genome was analysed from each sample.

Genomic diversity and population structure

To measure the amount of polymorphism within the parasite population, the average pairwise nucleotide diversity (π)among the sequences from the individual infection samples was calculated. The skewness in allele frequency distributions was estimated by Tajima's *D* index. Both indices were calculated using the same genome-wide SNP dataset in non-overlapping window sizes of 10 kb and performed using the DivStat software (Soares *et al.*, 2015). To illustrate the population substructure, the matrix of pairwise DNA distance among individuals was calculated and the Neighbour-Joining tree was constructed using the APE package version 3.4 in the R environment (Paradis *et al.*, 2004). An independent population structure evaluation was also conducted using principal coordinate analysis (PCoA) with SNPs having no missing data, using the APE package.

To estimate the divergence between the subpopulations, the genome-wide distribution of the fixation index (F_{ST}) between the two-subpopulation clusters was computed with SNPs having minor allele frequencies (MAFs) above 0.1, and above 0.3, using customised R functions. An elevated F_{ST} threshold was set at the 90th percentile of the F_{ST} distributions for all SNPs. Average F_{ST} values were calculated in windows of 500 SNPs with sliding by 250 SNPs. The F_{ST} values for each window were tested for high- or low- differentiated regions against the genome-wide mean F_{ST} value.

Genomic regions with contrasting levels of inter-cluster divergence were determined empirically by examining the F_{ST} distribution across the genome at two different MAFs (MAF above 0.1 and 0.3). For each MAF analysis, average F_{ST} values were calculated in windows of 200 SNPs (sliding by 100 SNPs), 500 SNPs (sliding by 250 SNPs) and 1000 SNPs (sliding by 500 SNPs). Mean global F_{ST} values and window F_{ST} values were then converted into standard *z*-scores in order to standardise the definition of outlier windows for different parameters. Regions of high- or low-F_{ST} windows were observed and compared among the analyses that used different MAF parameters.

Genomic regions were categorised into low divergence regions (LDR; *z*-scores < -0.5), intermediate divergence regions (IDR), and high divergence regions (HDR; *z*-scores > 0.5). To determine the size of these regions in detail, adjacent outlier windows were merged to form larger adjoining regions. Peak and trough patterns of window *z*-scores around the thresholds (*z*-scores < -0.5 and *z*-scores > 0.5) were taken into consideration in determining the range of genomic regions. Each candidate region was demarcated by first and last SNPs that fell within the merged windows, except for HDRs where SNPs with elevated F_{ST} values were used as starting and end points.

Patterns of polymorphisms (nucleotide diversity summarised by π and allele frequency spectrum summarised by Tajima's *D*) in all genomic regions were evaluated using DivStat software. Test runs were performed in non-overlapping window sizes of 10-kb for each subpopulations. Nonparametric Kruskal-Wallis tests were used to test for differences among the genomic regions as well as against the genome-wide background.

Extra-chromosomal genomes

Population structure and phylogeny of the sympatric *P. knowlesi* subpopulations were further analysed using the extranuclear DNA, consisting of the genomes of mitochondria and plastid-like apicoplast. The 5.9-kb mitochondrial DNA sequences were obtained from the present whole genome sequence data and previously published sequences (Assefa *et al.*, 2015; Jongwutiwes *et al.*, 2005; Lee *et al.*, 2011; Pinheiro *et al.*, 2015). Complete mitochondrial sequences were obtained from Genbank database, consisting of 26 haplotypes from human isolates (accession numbers EU880446 – EU880470) and 20 haplotypes from macaque isolates (EU880471 – EU880474, EU880477 – EU880486, EU880489 – EU880493 and EU880499) in Kapit of Malaysian Borneo, and one human isolate from Thailand (AY598141). Three species, *P. coatneyi* (AB354575), *P. cynomolgi* (AB434919) and *P. vivax* (AY791551), that have evolutionary relationships with *P. knowlesi* were included in the analysis as outgroups. Each DNA sequence was manually checked for the correct orientation due to the circular form of the genome. For the apicoplast genome of *P. knowlesi*, 30.6-kb of the DNA sequences that had clear alignment were extracted from the present whole genome dataset as well as from previous data (Assefa *et al.*, 2015; Pinheiro *et al.*, 2015) following mapping and base quality checks as mentioned above.

The derived mitochondrial and apicoplast genome sequences were separately aligned using the ClustalX programme version 2 (Larkin *et al.*, 2007), following which nucleotide diversity (π) and haplotype diversity (*Hd*) was determined using the DnaSP version 5 software (Librado and Rozas, 2009). A maximum likelihood tree was inferred with 1,000 bootstrap replicates and gaps treated as missing data using the *phangorn* packages in R (Schliep, 2011), with the ModelTest algorithm used to determine the best-fit nucleotide substitution model, which was GTR+I+G (General Time Reversible model with a proportion of invariable sites and gamma distribution). For the mitochondrial sequences, major haplotypes were determined with gaps treated as missing data, and the statistical parsimony haplotype network was constructed using the TCS version 1.21 software (Clement *et al.*, 2000).

Results

Generation of new whole-genome sequences and SNP genotyping

Paired-end Illumina sequencing of 21 new *P. knowlesi* clinical infection samples, selected on the basis of microsatellite genotyping as belonging to Cluster 2 (the type previously associated with pig-tailed macaque as well as human infections), yielded a mean of 6.95 million high quality reads per sample, which were mapped against the *P. knowlesi* H strain version 2.0 reference genome sequence (Table S3, Supporting information). The mean depth of sequence coverage genome-wide was 52.3 fold (range from 28.7 to 80.3 fold) per sample. Given a high quality of sequence coverage and single nucleotide polymorphism (SNP) calling, all samples were used for analyses. In addition, Illumina short read sequence data from another 59 *P. knowlesi* isolates obtained previously (Assefa *et al.*, 2015; Pinheiro *et al.*, 2015) were remapped against the *P. knowlesi* H strain version 2.0 reference genome using the same assembly parameters (Table S1, Supporting information). In the combined dataset of 80 infection sequences, a total of 2,109,937 SNPs were identified in the nuclear genome. Following exclusion of those in subtelomeric regions or in the *KIR* or *SICAVAR* multigene families, or that had more than two alleles, 1,669,533 SNPs remained, of which 1,186,073 high quality SNPs with less than 10% missing calls among all isolates were used for population genomic analyses.

Population genetic structure

Consistent with predictions from cluster assignment based on microsatellite genotyping, all 21 of the new *P. knowlesi* clinical infection samples showed genome sequences belonging to Cluster 2 (Fig. 1A; Fig. S1, Supporting information). Together with previous data, this yielded an overall sample of 34 Cluster 2 isolate sequences, to achieve a similar sample size as previously available for Cluster 1. As is visually apparent from the Neighbour-Joining tree based on the pairwise genetic distances (Fig. 1A), the Cluster 2 infections are less genetically diverse ($\pi = 3.43 \times 10^{-3}$) than the Cluster 1 infections ($\pi = 5.78 \times 10^{-3}$). Furthermore, the Cluster 1 subpopulation demonstrated a homogenous pattern of sequence diversity across the 14 chromosomes (Kruskal-Wallis, $P = 0.23$), in contrast with Cluster 2 that showed heterogeneous levels of diversity across the chromosomes (Kruskal-Wallis $P < 10^{-16}$) (Fig. S2, Supporting information). In Cluster 2, nucleotide diversity of entire chromosomes ranged from 2.25×10^{-3} (for chromosome 7) to 4.38×10^{-3} (for chromosome 5), but all had a lower diversity than in Cluster 1 (Wilcoxon Signed Rank $P < 10^{-16}$). In a majority of non-overlapping 10 kb windows genome-wide, nucleotide diversity (π) indices were lower in Cluster 2 (Fig. 1B). Large regions of chromosomes showed contiguous stretches in which diversity was much higher in Cluster 1, and also contiguous stretches in which the diversity was more similar (Fig. 1C)

Genomic regions of high and low divergence

The genome-wide variation in diversity in Cluster 2 suggested that there might be variation in levels of inter-cluster divergence. Analysing SNPs with overall minor allele frequencies above 10% (193,068 SNPs), the mean genome-wide fixation index indicated substantial divergence between the two subpopulations (mean $F_{ST} = 0.25$; Fig. 2A). The frequency distribution of F_{ST} values was bimodal, one peak having values just above zero and a second peak having values at or approaching 1.0 (Fig. 2B). Very high inter-cluster F_{ST} values of > 0.8 were seen for 19,116 SNPs, and 7,415 (3.8%) showed complete fixation of alternative alleles (F_{ST} = 1.0). A large proportion of low F_{ST} values were removed when analysis focused on SNPs with overall allele frequencies of > 0.3, showed similar proportions of SNPs with F_{ST} values at or near zero and 1.0 (Fig. 2B). Mean F_{ST} values for whole chromosomes ranged from 0.09 (for chromosome 5) to 0.40 for (chromosome 7).

The relative level of population differentiation of all windows of 500 contiguous SNPs across the genome was evaluated by calculating standard deviations from the mean genome-wide F_{ST} (*z*-score). Genomic regions were identified that contained contiguous windows defining low divergence regions (LDR with *z*-score < -0.5) and high divergence regions (HDR with *z*-score > 0.5). This revealed large genomic blocks of high or low divergence (Fig. 2C; Table S4, Supporting information). For example, chromosomes 7, 12 and 13 had HDRs covering most of their respective lengths, whereas chromosomes 3, 5 and 10 showed no HDRs (Fig. 2C).

Intra-cluster diversity in genomic regions with contrasting levels of divergence

The relationship with the varying nucleotide diversity (π) in cluster 2 across the genome (Fig. 1C) was investigated. Comparing between the two subpopulations, the differences in nucleotide diversity were higher in the HDRs than in the LDRs or in the rest of the genome (Fig. 3; Mann-Whitney U P < 10^{-16} for both comparisons). Most of the highly differentiated regions were those in which nucleotide diversity was substantially lower in Cluster 2 (Fig. 3).

Reduced nucleotide diversity in HDRs compared to the rest of the genome was specifically seen in Cluster 2 (mean π in HDRs = 2.08 x 10^{-3}; Mann-Whitney P < 2.2 x 10^{-16}), and not in Cluster 1 (mean π in HDRs = 5.80 x 10^{-3}; Mann-Whitney P = 0.25). Similarly, higher nucleotide diversity in LDRs compared to the rest of the genome was seen specifically within cluster 2 (Mann-Whitney P = 2.2 x 10^{-16}), and not in Cluster 1 (Mann-Whitney P = 0.77).

Both subpopulations showed strong skew towards low frequency variants, with mean Tajima's *D* values for the Cluster 2 subpopulation being even lower than for the Cluster 1 subpopulation (Fig. 4A; Cluster 1 mean *D* = -1.77; Cluster 2 mean *D* = -2.37; Wilcoxon Signed Rank $P < 10^{-16}$). Across all 10 kb windows in the genome, there was a weak but highly significant correlation in the distribution of Tajima's *D* values (Fig. 4B; Spearman's rho = 0.25; $P < 10^{-16}$). The allele frequency spectrum as summarized by Tajima's D index was less variable across the 14 chromosomes within the Cluster 1 subpopulation (Kruskal-Wallis $P = 8.4 \times 10^{-5}$) compared to the Cluster 2 subpopulation (Kruskal-Wallis $P = 1.6 \times 10^{-16}$) (Fig. 4C).

The mosaic pattern of genomic diversity in the Cluster 2 subpopulation suggests that a scan to identify individual genes with exceptionally high values of Tajima's D may not be a robust means of identifying genes under balancing selection in this subpopulation, although the approach was more straightforwardly applied to the Cluster 1 subpopulation previously (Assefa *et al.*, 2015). However, the *msp1* merozoite surface protein antigen gene that was previously shown to have a high Tajima's D value in Cluster 1 also had a high value in the Cluster 2 subpopulation (*D* = 1.01). Interestingly, the *ama1* apical membrane antigen gene that did not have a high value in Cluster 1 had an exceptionally high value in Cluster 2 here (*D* = 1.64). The *csp* circumsporozoite protein gene, that had the highest Tajima's *D* value of all genes in Cluster 1, did not have any detected non-repeat sequence polymorphisms in Cluster 2. Thus, although an unbiased comparison cannot be straightforwardly performed, these examples indicate that there may be differences in the strength or targets of balancing selection on antigens in the two different parasite subpopulations.

Phylogeny and introgression of extra-chromosomal genomes

The analyses of population structure was extended using the maternally inherited extra-chromosomal genomes. Combination of the 5.9 kb mitochondrial sequences generated in this study with previously published sequences yielded a sample size of 129 in total, and identification of 77 SNPs. These mitochondrial sequences had a global average nucleotide diversity (π) of 7.9 x 10^{-4}, with higher values in samples from parasites in Cluster 1 (π = 6.8 x 10^{-4}, n = 74) than in Cluster 2 (π = 4.9 x 10^{-4}, n = 46). The genealogical network of mitochondrial genomes contained 56 different haplotypes (Fig. 5). The most common and central core haplotype was detected mainly in parasites of the Cluster 1 subpopulation (25 out of 28 isolates). A second common haplotype that was more peripheral in the network was seen mostly in the Cluster 2 subpopulation (15 out of 21 isolates), while the third common haplotype was distantly related to this and detected only in Cluster 1 (9 isolates). Most of the closely related haplotypes to each of these were also seen only in the corresponding subpopulation clusters, but there is a group of closely related haplotypes internal in the network seen in parasites of Cluster 1 (13 isolates) which is embedded in part of the network that is otherwise only seen in Cluster 2 parasites (Fig. 5). Conversely, a few Cluster 2 isolates have haplotypes that are related to those only seen in Cluster 1. A separate branch of haplotypes was seen in laboratory isolates that had mostly been collected from Peninsular Malaysia, supporting the geographical divergence seen in the nuclear genomes. Maximum likelihood phylogenetic analysis yielded a similar pattern, with haplotype clades being associated but not completely fixed between the Cluster 1 and Cluster 2 subpopulations (Fig. S3; Supporting information).

Polymorphism in 30.6 kb of the apicoplast genome could be characterised using the Illumina short read sequence data to identify 520 polymorphic SNPs. With these data, 65 of the 80 isolates were analysed in detail as they had less than 20% missing SNPs, while the remaining 15 samples with more missing SNP data were excluded. The overall nucleotide diversity (π) was 1.79 x 10^{-3} , and this was higher among the Cluster 1 samples ($\pi = 1.77 \times 10^{-3}$) than Cluster 2 samples ($\pi = 1.12 \times 10^{-3}$). Two major lineages were seen, one of which consisted predominantly of Cluster 1 samples, and the other mainly of Cluster 2 samples (Fig. S4, Supporting information), although there were several isolates that had haplotypes of the opposite type to that expected for each cluster.

Discussion

This study analyses the largest ecological sample of sequences representing different subpopulations of a zoonotic eukaryotic parasite species. Whole genome sequencing of new samples from one of the major genetic subpopulations of *P. knowlesi* has clearly revealed the genome-wide patterns of divergence between the sympatric subpopulations, which illuminates aspects of their population history and is essential for understanding their adaptive potential. This provides the most informative overall analysis of population structure of *P. knowlesi* to date, extending the understanding of defined subpopulation clusters that were previously described (Assefa *et al.*, 2015; Divis *et al.*, 2017). These results confirm the distinctness of the two sympatric divergent *P. knowlesi* subpopulations in Malaysian Borneo, supporting the occurrence of independent zoonotic cycles associated with different macaque reservoir host species (Divis *et al.*, 2015; Muehlenbein *et al.*, 2015).

The high differentiation between these two sympatric subpopulations indicates limited gene flow occurring between them. A large number of SNPs showed complete fixation, even with the large sample size of Cluster 2 parasites obtained here. However, the pattern of divergence was heterogeneous and bimodally distributed with large regions of exceptionally high and low divergence interspersed throughout the genome. Reduced genetic diversity of the Cluster 2 subpopulation in highly diverged regions suggests there may have been an initial bottleneck in the formation of this subpopulation. The overall allele frequency spectra were negative skewed for both subpopulations, signifying long term population growth, although this was more extreme for the Cluster 2 subpopulation. This gives a more detailed perspective than that previously obtained by analysis of mitochondrial genome sequences, which first indicated a historical population expansion (Lee *et al.*, 2011). The mitochondrial and apicoplast genomes in *Plasmodium* are inherited together through the female parasite gamete in each transmission cycle (Lim and McFadden, 2010) with negligible recombination at the population level, but analyses of these extra-chromosomal genomes here indicates some sharing of different haplotypes between the *P. knowlesi* subpopulations. The mosaic pattern with adjacent large regions of alternating high and low diversity in the genome sequences of the Cluster 2 subpopulation, in contrast to the more consistent high diversity throughout the genome for the Cluster 1 subpopulation, suggests that introgression has probably occurred recently from Cluster 1 into the Cluster 2 population.

Despite the differences at the genomic level, it is not yet known whether these two major sympatric subpopulations exhibit significant phenotypic differences, apart from the previously described association with different macaque reservoir host species (Divis *et al.*, 2017; Divis *et al.*, 2015; Lee *et al.*, 2011). Human *P. knowlesi* infections have been associated with a wide spectrum of disease (Cox-Singh *et al.*, 2010; Daneshvar *et al.*, 2009; Rajahram *et al.*, 2012; William *et al.*, 2011), and there is recent evidence that asymptomatic infections may be more common than previously expected (Fornace *et al.*, 2015; Lubis *et al.*, 2017; Siner *et al.*, 2017), so conducting detailed clinical studies on individuals infected with each parasite subpopulation type is now a priority.

A recent study suggests a link between local deforestation and incidence of *P. knowlesi* infections in an area of Sabah state within Malaysian Borneo (Fornace *et al.*, 2016). Of relevance to this, long-tailed macaques and pig-tailed macaques show different habitat ranges in forested and non-forested areas (Moyes *et al.*, 2016), suggesting that there may be micro foci of infection for each subpopulation cluster, and highlighting the need to examine changes over time. It is clear that future research should include monitoring the proportions of the different *P. knowlesi* subpopulations over time, and potential changes in their genetic composition. Sequencing of *P. knowlesi* genomes from natural macaque infections would be more challenging, given that these are usually coinfections together with other primate malaria parasite species (Lee *et al.*, 2011), although new methods of sequencing genomes from single parasites could be adapted to address the issue (Trevino *et al.*, 2017). This would ideally be done alongside sampling of infections in local mosquito vector species that could potentially be maintaining the separate zoonotic transmission cycles.

The genome-wide mosaicism, showing bimodal levels of divergence as well as limited discordant occurrence of extrachromosomal genome lineages, indicate that introgression is likely to have occurred recently between these parasite subpopulations. The recombinant genomes that are now circulating offer a great diversity on which selection may operate, but there is no evidence yet of specific adaptation at introgressed loci. A recent re-analysis of previously published data identified a common shared haplotype in a chromosomal region with low divergence between the subpopulations (Diez Benavente *et al.*, 2017), although an observation that the region had a slightly higher than background proportion of genes predicted to be expressed at a particular developmental stage may not be relevant, as an extended haplotype may result from selection on a single locus rather than on multiple genes.

In contrast, it is likely that at least one of the chromosomal regions showing fixed differences between the clusters contains a locus responsible for maintaining genetic isolation of the sympatric subpopulations, potentially due to transmission in different mosquito vectors, as well as likely adaptation to the different reservoir macaque hosts. Parasites from these sympatric subpopulations have not yet been studied in laboratory infections or adapted to culture, which will be necessary to define phenotypes and enable experimental analyses of differences between them. Despite the major technical challenges of such work, the substantial efforts should prove worthwhile, as they are likely to reveal parasite adaptations beyond those identified using old laboratory lines sampled from a different part of the parasite species range (Dankwa *et al.*, 2016; Moon *et al.*, 2016). If there are no parasite subpopulation-specific barriers to infection of mosquito vectors that may be experimentally used, such as *Anopheles cracens* (Amir *et al.*, 2013), it should ultimately be possible to map loci controlling key phenotypes by performing genetic crosses between parental parasites representing the different subpopulations.

Acknowledgments

We are grateful to all patients, nurses and clinical staff at Kapit Hospital who provided and collected samples for this study, and the laboratory technicians at Kapit Hospital Pathology Laboratory for processing the blood samples. We thank the Director General of Health Malaysia for permission to publish this paper. We also thank colleagues in Malaria Research Centre, Universiti Malaysia Sarawak and London School of Hygiene and Tropical Medicine for laboratory assistance. This study was supported by grants 01/(TD03)/1003/2012(01) and F05/SpTDG/1447/2016/4 from UNIMAS, and AdG-2011-294428 from the European Research Council, as well as a postgraduate scholarship from Ministry of Higher Education in Malaysia.

References

Amir A, Sum JS, Lau YL, Vythilingam I, Fong MY (2013) Colonization of *Anopheles cracens*: a malaria vector of emerging importance. *Parasit Vectors* **6**, 81.

Assefa S, Lim C, Preston MD*, et al.* (2015) Population genomic structure and adaptation in the zoonotic malaria parasite *Plasmodium knowlesi*. *Proc Natl Acad Sci U S A* **112**, 13027-13032.

Barber BE, Rajahram GS, Grigg MJ, William T, Anstey NM (2017) World Malaria Report: time to acknowledge *Plasmodium knowlesi* malaria. *Malar J* **16**, 135.

Bolger AM, Lohse M, Usadel B (2014) Trimmomatic: a flexible trimmer for Illumina sequence data. *Bioinformatics* **30**, 2114-2120.

Clement M, Posada D, Crandall KA (2000) TCS: a computer program to estimate gene genealogies. *Mol Ecol* **9**, 1657-1659.

Coatney GR, Collin WE, Warren M, Contacos PG (1971) *The Primate Malarias* U.S. Government Printing Office, Washington.

Cox-Singh J, Davis TM, Lee KS*, et al.* (2008) *Plasmodium knowlesi* malaria in humans is widely distributed and potentially life threatening. *Clin Infect Dis* **46**, 165-171.

Cox-Singh J, Hiu J, Lucas SB*, et al.* (2010) Severe malaria - a case of fatal *Plasmodium knowlesi* infection with post-mortem findings: a case report. *Malar J* **9**, 10.

Daneshvar C, Davis TM, Cox-Singh J*, et al.* (2009) Clinical and laboratory features of human *Plasmodium knowlesi* infection. *Clin Infect Dis* **49**, 852-860.

Dankwa S, Lim C, Bei AK*, et al.* (2016) Ancient human sialic acid variant restricts an emerging zoonotic malaria parasite. *Nat Commun* **7**, 11187.

Diez Benavente E, Florez de Sessions P, Moon RW*, et al.* (2017) Analysis of nuclear and organellar genomes of *Plasmodium knowlesi* in humans reveals ancient population structure and recent recombination among host-specific subpopulations. *PLoS Genet* **13**, e1007008.

Divis PC, Lin LC, Rovie-Ryan JJ*, et al.* (2017) Three divergent subpopulations of the malaria parasite *Plasmodium knowlesi*. *Emerg Infect Dis* **23**, 616-624.

Divis PC, Singh B, Anderios F*, et al.* (2015) Admixture in humans of two divergent *Plasmodium knowlesi* populations associated with different macaque host species. *PLoS Pathog* **11**, e1004888.

Fornace KM, Abidin TR, Alexander N*, et al.* (2016) Association between landscape factors and spatial patterns of *Plasmodium knowlesi* infections in Sabah, Malaysia. *Emerg Infect Dis* **22**, 201-208.

Fornace KM, Nuin NA, Betson M*, et al.* (2015) Asymptomatic and submicroscopic carriage of *Plasmodium knowlesi* malaria in household and community members of clinical cases in Sabah, Malaysia. *J Infect Dis* **213**, 784-787.

Jongwutiwes S, Putaporntip C, Iwasaki T*, et al.* (2005) Mitochondrial genome sequences support ancient population expansion in *Plasmodium vivax*. *Mol Biol Evol* **22**, 1733-1739.

Larkin MA, Blackshields G, Brown NP*, et al.* (2007) Clustal W and Clustal X version 2.0. *Bioinformatics* **23**, 2947-2948.

Lee KS, Divis PC, Zakaria SK*, et al.* (2011) *Plasmodium knowlesi*: reservoir hosts and tracking the emergence in humans and macaques. *PLoS Pathog* **7**, e1002015.

Li H (2013) Aligning sequence reads, clone sequences and assembly contigs with BWA-MEM. *arXivorg*, arXiv:1303.3997v1302 [q-bio.GN].

Li H, Handsaker B, Wysoker A*, et al.* (2009) The Sequence Alignment/Map format and SAMtools. *Bioinformatics* **25**, 2078-2079.

Librado P, Rozas J (2009) DnaSP v5: a software for comprehensive analysis of DNA polymorphism data. *Bioinformatics* **25**, 1451-1452.

Lim C, Hansen E, DeSimone TM*, et al.* (2013) Expansion of host cellular niche can drive adaptation of a zoonotic malaria parasite to humans. *Nat Commun* **4**, 1638.

Lim L, McFadden GI (2010) The evolution, metabolism and functions of the apicoplast. *Philos Trans R Soc Lond B Biol Sci* **365**, 749-763.

Lubis IN, Wijaya H, Lubis M*, et al.* (2017) Contribution of *Plasmodium knowlesi* to multi-species human malaria infections in North Sumatera, Indonesia. *J Infect Dis*.

Moon RW, Hall J, Rangkuti F*, et al.* (2013) Adaptation of the genetically tractable malaria pathogen *Plasmodium knowlesi* to continuous culture in human erythrocytes. *Proc Natl Acad Sci U S A* **110**, 531-536.

Moon RW, Sharaf H, Hastings CH*, et al.* (2016) Normocyte-binding protein required for human erythrocyte invasion by the zoonotic malaria parasite Plasmodium knowlesi. *Proc Natl Acad Sci U S A* **113**, 7231-7236.

Moyes CL, Shearer FM, Huang Z*, et al.* (2016) Predicting the geographical distributions of the macaque hosts and mosquito vectors of *Plasmodium knowlesi* malaria in forested and non-forested areas. *Parasit Vectors* **9**, 242.

Muehlenbein MP, Pacheco MA, Taylor JE*, et al.* (2015) Accelerated diversification of nonhuman primate malarias in southeast Asia: adaptive radiation or geographic speciation? *Mol Biol Evol* **32**, 422-439.

Pain A, Bohme U, Berry AE*, et al.* (2008) The genome of the simian and human malaria parasite *Plasmodium knowlesi*. *Nature* **455**, 799-803.

Paradis E, Claude J, Strimmer K (2004) APE: Analyses of Phylogenetics and Evolution in R language. *Bioinformatics* **20**, 289-290.

Pinheiro MM, Ahmed MA, Millar SB*, et al.* (2015) *Plasmodium knowlesi* genome sequences from clinical isolates reveal extensive genomic dimorphism. *PLoS One* **10**, e0121303.

Quinlan AR, Hall IM (2010) BEDTools: a flexible suite of utilities for comparing genomic features. *Bioinformatics* **26**, 841-842.

Rajahram GS, Barber BE, William T*, et al.* (2016) Falling *Plasmodium knowlesi* malaria death rate among adults despite rising incidence, Sabah, Malaysia, 2010-2014. *Emerg Infect Dis* **22**, 41-48.

Rajahram GS, Barber BE, William T*, et al.* (2012) Deaths due to *Plasmodium knowlesi* malaria in Sabah, Malaysia: association with reporting as *Plasmodium malariae* and delayed parenteral artesunate. *Malar J* **11**, 284.

Schliep KP (2011) phangorn: phylogenetic analysis in R. *Bioinformatics* **27**, 592-593.

Siner A, Liew ST, Kadir KA*, et al.* (2017) Absence of *Plasmodium inui* and *Plasmodium cynomolgi*, but detection of *Plasmodium knowlesi* and *Plasmodium vivax* infections in asymptomatic humans in the Betong division of Sarawak, Malaysian Borneo. *Malar J* **16**, 417.

Singh B, Daneshvar C (2013) Human infections and detection of *Plasmodium knowlesi*. *Clin Microbiol Rev* **26**, 165-184.

Singh B, Kim Sung L, Matusop A*, et al.* (2004) A large focus of naturally acquired *Plasmodium knowlesi* infections in human beings. *Lancet* **363**, 1017-1024.

Soares I, Moleirinho A, Oliveira GN, Amorim A (2015) DivStat: a user-friendly tool for single nucleotide polymorphism analysis of genomic diversity. *PLoS One* **10**, e0119851.

Trevino SG, Nkhoma SC, Nair S*, et al.* (2017) High-resolution single-cell sequencing of malaria parasites. *Genome Biol Evol* **Epub before print.**

William T, Menon J, Rajahram G*, et al.* (2011) Severe *Plasmodium knowlesi* malaria in a tertiary care hospital, Sabah, Malaysia. *Emerg Infect Dis* **17**, 1248-1255.

William T, Rahman HA, Jelip J*, et al.* (2013) Increasing incidence of *Plasmodium knowlesi* malaria following control of *P. falciparum* and *P. vivax* malaria in Sabah, Malaysia. *PLoS Negl Trop Dis* **7**, e2026.

Yusof R, Ahmed MA, Jelip J*, et al.* (2016) Phylogeographic evidence for 2 genetically distinct zoonotic *Plasmodium knowlesi* parasites, Malaysia. *Emerg Infect Dis* **22**, 1371-1380.

Yusof R, Lau YL, Mahmud R*, et al.* (2014) High proportion of knowlesi malaria in recent malaria cases in Malaysia. *Malar J* **13**, 168.

Data Accessibility Statement

Paired-end short read genome sequence data for the new parasite infection isolates listed in Supplementary Table S3 have been deposited in the European Nucleotide Archive, accession numbers ERS2037781-ERS2037801.

Author contributions

PCSD, BS and DJC conceived and designed the study. KAK and BS collected and prepared the samples. PCSD conducted the genome sequencing, bioinformatic SNP calling and nucleotide data deposition. PCSD, CWD and DJC performed data analysis and interpretation. PCSD and DJC wrote the manuscript, with input from all authors.

Figure Legends

Fig. 1. Population structure of *P. knowlesi* indicated by whole genome sequence data. (A) Neighbour-Joining tree based on a pairwise SNP difference matrix of 80 *P. knowlesi* isolates. The 21 new genome sequences are indicated with stars, yielding a total sample size for Cluster 2 (N=34) that is similar to that of Cluster 1 (N=41). The scale bar indicates proportions of all SNPs differing between samples. (B) Scatterplot of nucleotide diversity (π) in individual non-overlapping 10 kb windows of the genome, comparing data for Cluster 1 and Cluster 2 subpopulations. (C) Differences in nucleotide diversity between Cluster 1 and Cluster 2 subpopulations (*π*-diff) in each of the 10 kb windows of the genome.

Fig. 2. Genome-wide plot of divergence between the sympatric *P. knowlesi* Cluster 1 and Cluster 2 subpopulations in Malaysian Borneo. Each dot shows the F_{ST} value of an individual SNP, out of 193,068 SNPs with minor allele frequencies above 0.1. The overall genome-wide mean F_{ST} value is 0.25. (B) Strong bimodal frequency distribution of F_{ST} values for SNPs genome-wide. The left plot shows the distribution of values for 193,068 SNPs with minor allele frequencies (MAF) > 0.1, and the right plot shows the distribution of values for 80,168 SNPs with MAF > 0.3 (the genome-wide average F_{ST} value was 0.42 for SNPs with MAF > 0.3). (C) Contiguous regions of high and low divergence throughout the genome identified by analysis of F_{ST} values of windows of 500 consecutive SNPs converted to standardised z-scores. Thresholds of 0.5 standard deviations above and below the genome-wide average F_{ST} demarcate the regions of high divergence (red blocks) and low divergence (dark blue blocks).

Fig. 3. Sequence diversity of *P. knowlesi* Cluster 2 is lowest in regions of the genome that have highest fixation indices in comparison with Cluster 1. Scatterplots show nucleotide diversity in discrete 10 kb windows genome-wide, with red points (left) showing windows in high divergence regions (HDR) and blue points showing windows in low divergence regions (LDR). For HDR, mean π = 5.80×10^{-3} for Cluster 1 and 2.08×10^{-3} for Cluster 2. For LDR, mean $\pi = 5.60 \times 10^{-3}$ for Cluster 1 and 4.14×10^{-3} for Cluster 2.

Fig. 4. Comparison of genome-wide Tajima's *D* distributions between the two major *P. knowlesi* genetic subpopulations in Malaysian Borneo. (A) Frequency distribution of Tajima's *D* values in non-overlapping 10 kb windows for Cluster 2 shows more negatively skewed values compared to Cluster 1. (B) Tajima's *D* values for individual 10 kb windows show a weak correlation between the two subpopulations (Spearman's ρ = 0.25), although this is highly significant ($P < 10^{-16}$). (C) Distribution of Tajima's *D* values in non-overlapping 10 kb windows across all 14 chromosomes presented in

alternate dark and light grey blocks. The mean genome-wide value for Cluster 1 is -1.77 and for Cluster 2 is -2.37.

Fig. 5. Genealogical network based on 129 *P. knowlesi* mitochondrial DNA genome sequences showing 56 different haplotypes. Sizes of the circles represent relative numbers of samples with each haplotype, with numbers specified where this is more than one. Connecting lines each represent one mutational step and black dots represent missing intermediate haplotypes.

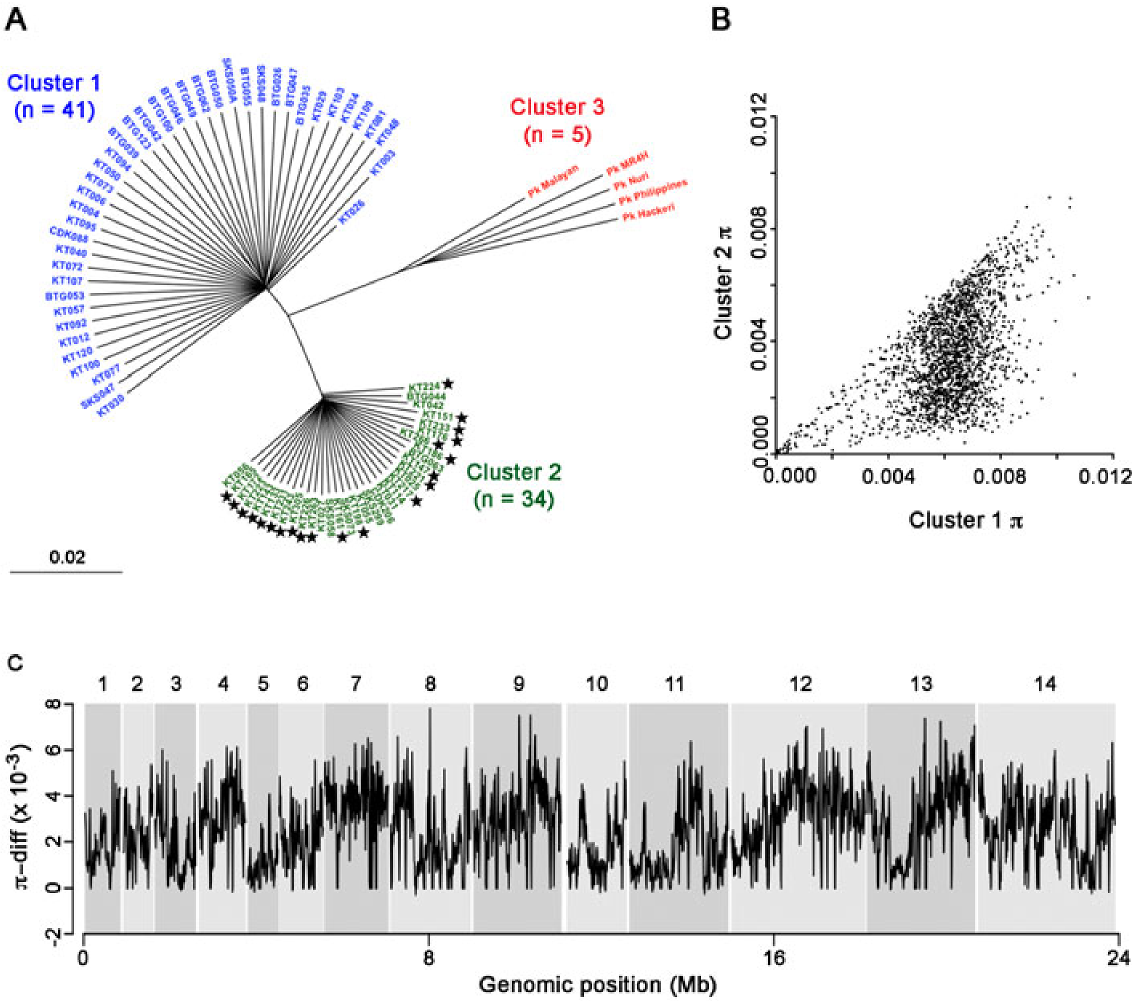
A
Cluster 1
(n = 41)
KT030
SKS047
KT077
KT100
KT120
KT012
KT092
KT057
BTG053
KT107
KT072
KT040
CDK088
KT095
KT004
KT006
KT073
KT050
KT094
BTG039
BTG123
BTG042
BTG100
BTG046
BTG049
BTG062
BTG050
SKS050A
BTG055
SKS048
BTG026
BTG047
BTG035
KT029
KT103
KT034
KT109
KT081
KT048
KT003
KT026
Cluster 3
(n = 5)
Pk Malayan
Pk MR4H
Pk Nuri
Pk Philippines
Pk Hackeri
KT224
BTG044
KT042
KT151
KT233
Cluster 2
(n = 34)
0.02
B
Cluster 2 π
0.000
0.004
0.008
0.012
Cluster 1 π
0.000
0.004
0.008
0.012
C
1
2
3
4
5
6
7
8
9
10
11
12
13
14
π-diff (x 10⁻³)
-2
0
2
4
6
8
0
8
16
24
Genomic position (Mb)

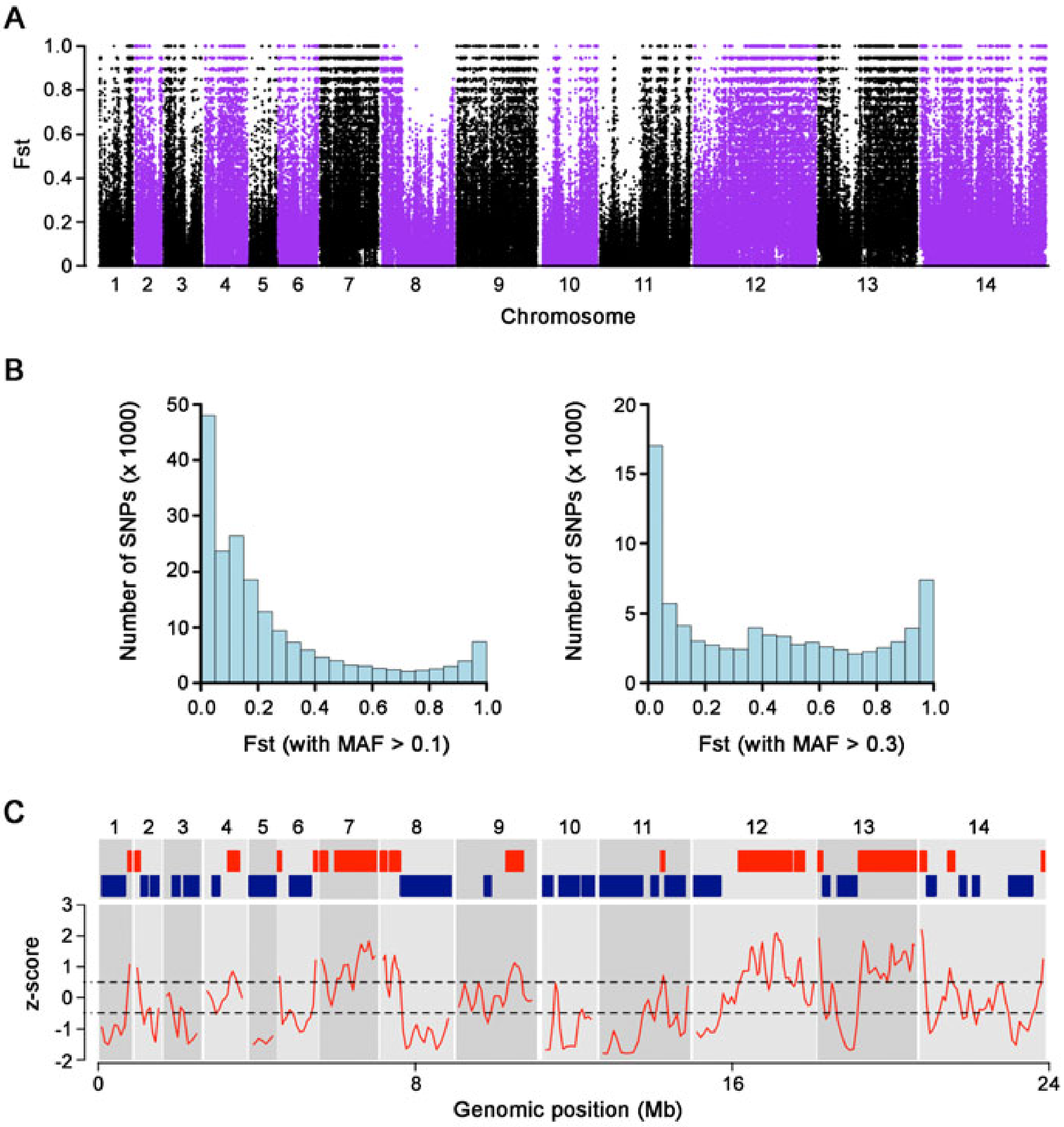
A
Fst
1.0
0.8
0.6
0.4
0.2
0
1
2
3
4
5
6
7
8
9
10
11
12
13
14
Chromosome
B
Number of SNPs (x 1000)
50
40
30
20
10
0
0.0
0.2
0.4
0.6
0.8
1.0
Fst (with MAF > 0.1)
Number of SNPs (x 1000)
20
15
10
5
0
Fst (with MAF > 0.3)
C
z-score
3
2
1
0
-1
-2
0
8
16
24
Genomic position (Mb)

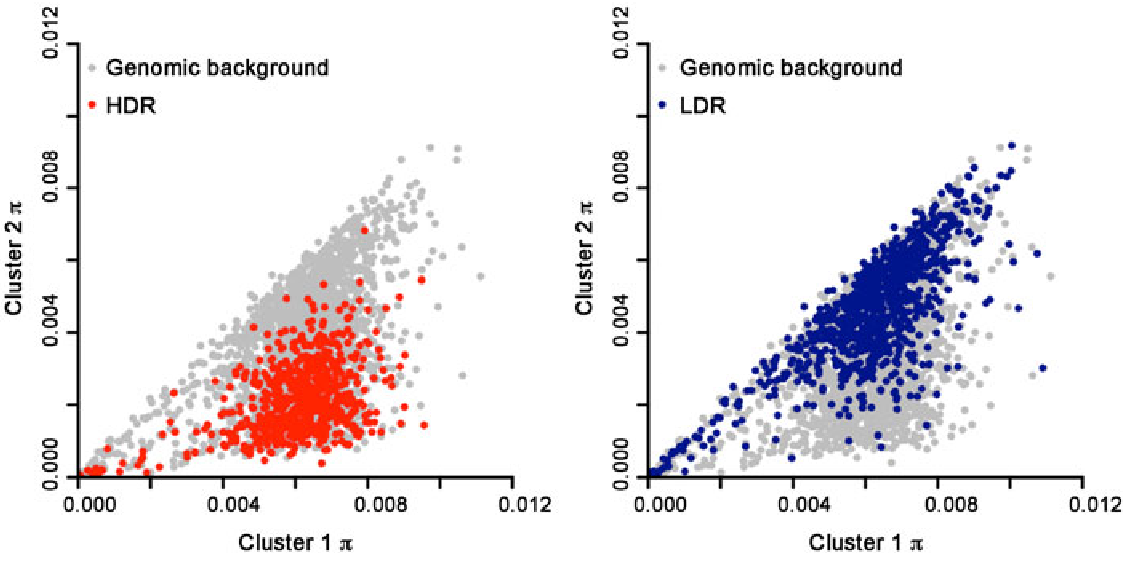
Genomic background
HDR
Cluster 2 π
Cluster 1 π
0.000
0.004
0.008
0.012
0.000
0.004
0.008
0.012
Genomic background
LDR
Cluster 2 π
Cluster 1 π
0.000
0.004
0.008
0.012
0.000
0.004
0.008
0.012

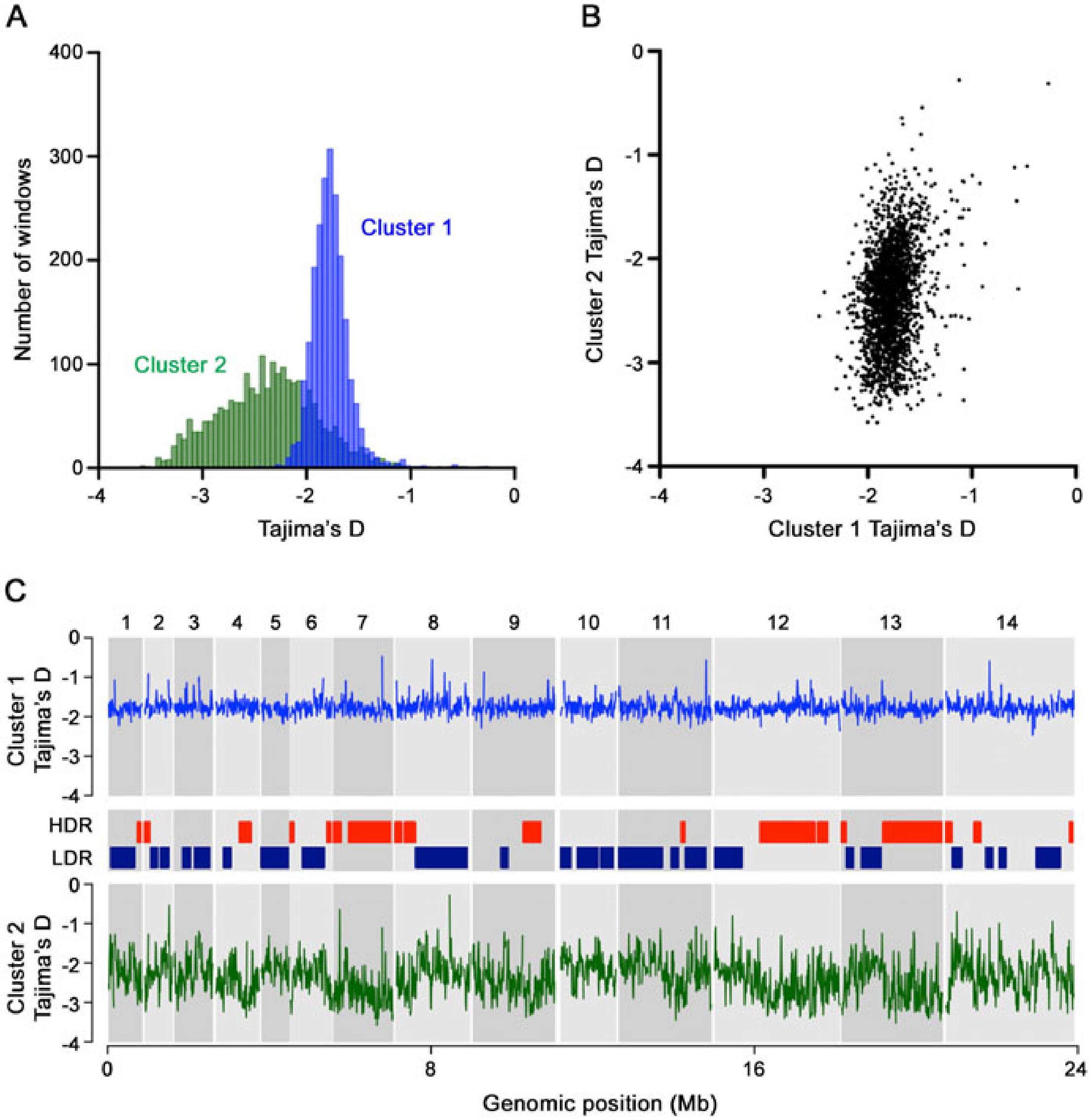
A
400
300
200
100
0
Number of windows
Cluster 1
Cluster 2
-4
-3
-2
-1
0
Tajima's D
B
0
-1
-2
-3
-4
Cluster 2 Tajima's D
-4
-3
-2
-1
0
Cluster 1 Tajima's D
C
1
2
3
4
5
6
7
8
9
10
11
12
13
14
0
-1
-2
-3
-4
Cluster 1 Tajima's D
HDR
LDR
0
-1
-2
-3
-4
Cluster 2 Tajima's D
0
8
16
24
Genomic position (Mb)

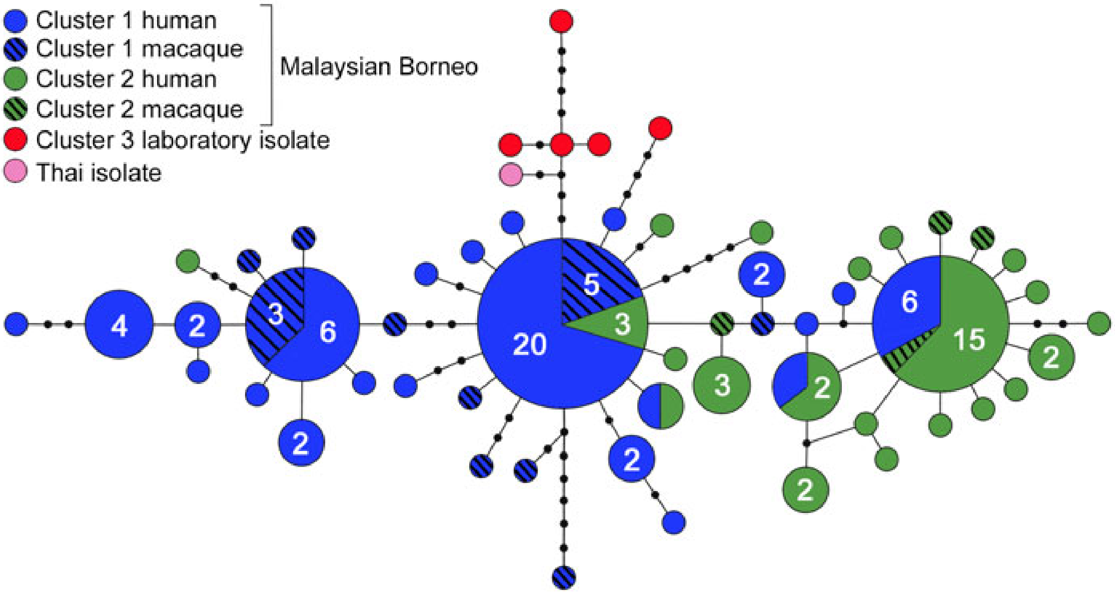
Cluster 1 human
Cluster 1 macaque
Cluster 2 human
Cluster 2 macaque
Cluster 3 laboratory isolate
Thai isolate
Malaysian Borneo
4
2
3
6
2
20
5
3
2
3
2
2
2
6
15
2
2